



PixelPonder: Dynamic Patch Adaptation for Enhanced Multi-Conditional Text-to-Image Generation

Yanjie Pan^{1*} Qingdong He^{2*} Zhengkai Jiang³ Pengcheng Xu⁴ Chaoyi Wang⁵ Jinlong Peng²
 Haoxuan Wang¹ Yun Cao² Zhenye Gan² Mingmin Chi^{1†} Bo Peng¹ Yabiao Wang²

¹Fudan University ²Youtu Lab, Tencent ³Hong Kong University of Science and Technology

⁴Western University ⁵University of Chinese Academy of Sciences

<https://hithqd.github.io/projects/PixelPonder/>

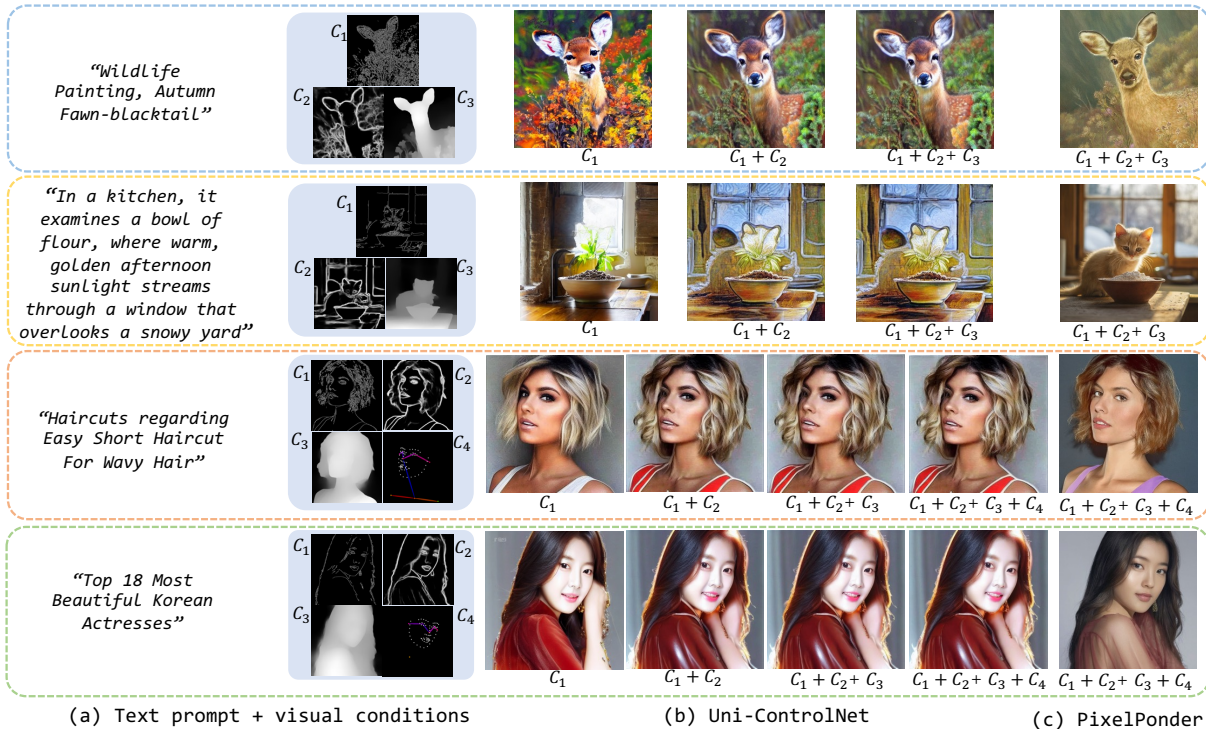


Figure 1. **Visualization comparison between Uni-ControlNet [51] and our proposed method in different conditional controls with the same text prompt.** (a, left two columns) Text and various visual controls, where C_1 , C_2 , C_3 and C_4 denotes edge, sketch, depth and pose map respectively. (b, middle three or four columns) Generation results from UniControlNet. (c, last column) Generation results from our PixelPonder. Previous methods struggled to generate coherent results under multiple conditions, while our results maintain strong similarity to the respective visual controls.

Abstract

Recent advances in diffusion-based text-to-image generation have demonstrated promising results through visual condition control. However, existing ControlNet-like methods struggle with compositional visual conditioning - simultaneously preserving semantic fidelity across multiple heterogeneous control signals while maintaining high visual quality, where they employ separate control branches that

often introduce conflicting guidance during the denoising process, leading to structural distortions and artifacts in generated images. To address this issue, we present PixelPonder, a novel unified control framework, which allows for effective control of multiple visual conditions under a single control structure. Specifically, we design a patch-level adaptive condition selection mechanism that dynamically prioritizes spatially relevant control signals at the sub-region level, enabling precise local guidance without global interference. Additionally, a time-aware control injection scheme is deployed to modulate condition influence accord-

* Equal contribution † Corresponding author

ing to denoising timesteps, progressively transitioning from structural preservation to texture refinement and fully utilizing the control information from different categories to promote more harmonious image generation. Extensive experiments demonstrate that PixelPonder surpasses previous methods across different benchmark datasets, showing superior improvement in spatial alignment accuracy while maintaining high textual semantic consistency.

1. Introduction

The emergence of diffusion-based text-to-image synthesis [9, 25, 26, 29, 30, 32] have driven significant progress in single-modality conditioned generation frameworks [4, 20–22, 48]. While these approaches demonstrate enhanced controllability through visual-textual alignment, fundamental limitations persist due to modality-specific biases in visual conditioning. As evidenced in [11, 35], distinct visual control signals exhibit complementary yet conflicting characteristics, such as depth maps effectively regulate inter-object spatial relationships but lack fine-grained object details, whereas canny maps capture precise texture contours while disregarding global structural context. This modality specialization gap raises a critical challenge: *How to establish an effective fusion paradigm for multi-visual condition control that synergistically integrates heterogeneous visual features (e.g., structural priors, textural details) while resolving inter-modality conflicts?*

In prior research endeavors, numerous advanced methods for single visual condition control [4, 23, 49] have been developed, yielding promising results in controllable image generation. Building upon this foundation, subsequent studies [22, 27, 51] have investigated unified approaches for single visual condition control generation. These methods successfully integrate various image condition controls into a single model, thereby accomplishing the goal of multi-category visual independent control generation using a unified framework. Despite these advancements, there have been few efforts to extend these methods to jointly control image generation with multiple visual conditions, yielding some positive outcomes. Furthermore, the prevalent strategy of leveraging prior knowledge from the control branches of each visual condition for simple combinations of visual conditions presents significant challenges. As illustrated in Fig. 1, generating normal images under complex, highly coupled visual condition controls remains a difficult task.

In practical applications, it is often necessary to describe the visual features of a significant object using multiple visual conditions to achieve precise control over its generation. Users typically desire to simultaneously control both the layout and the intricate details of the key target object. However, visual conditions that are rich in layout and de-

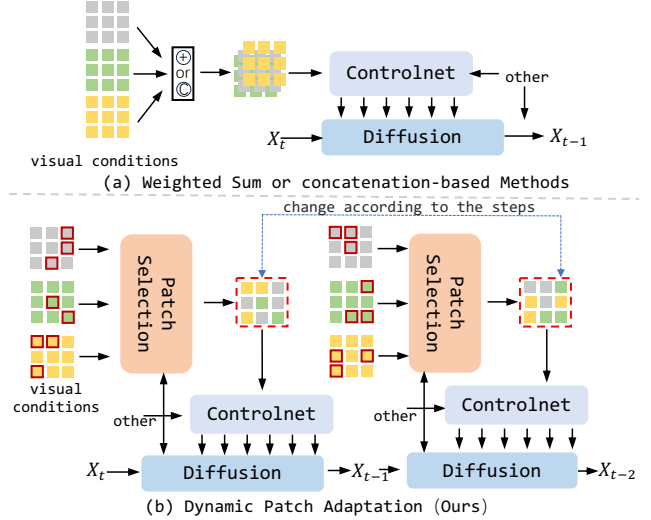


Figure 2. **Comparison of different schemes dealing with multiple condition.** (a) Existing methods integrate various visual controls into a highly consistent visual control signal in the temporal domain through concatenation or weighted summation. (b) We employ dynamic patch selection to reconstruct visual conditions at the patch level while preserving the regional features of each visual condition in the temporal domain, enabling multi-visual controllable generation in the generative model.

tail information are challenging to integrate into a single visual condition map. A common scenario involves using canny maps to represent details and depth maps to control the layout. In such case, these visual conditions are highly coupled, overlapping, and complementary to one another.

Bridging the conflicting information among these visual conditions and reasonably utilizing the emphasis of various visual conditions to coordinate the generation of the object is exactly the issue that this paper wants to focus on. As shown in Fig. 2(a), prior efforts including Cocktail [16] and Uni-ControlNet [51] propose to consolidate various visual conditions into unified latent representations. While this coarse-grained unification alleviates inter-condition conflicts through dimensionality reduction, it remains suboptimal in preserving modality-specific attributes critical for precise control (e.g., high-frequency textures in canny vs. low-frequency structures in depth). The inherent information bottleneck induced by latent compression disproportionately attenuates complementary cross-modal features, fundamentally limiting their capacity to synergize discriminative visual cues. This constitutes a critical limitation: current unification paradigms prioritize conflict mitigation over inter-modal feature reinforcement.

To address the aforementioned challenges, we introduce an innovative visual condition combination method termed *PixelPonder*. As illustrated in Fig. 2(b), our method distinguishes itself from previous approaches by integrating diverse visual conditions at the patch level. Recognizing that visual conditions enriched with low-frequency or high-

frequency signals significantly influence various denoising stages during the image generation process [15], we have developed an adaptive patch selection mechanism that dynamically adjusts with timesteps. This mechanism decouples each visual condition in the temporal domain, enabling the use of distinct combinations of visual conditions to regulate the denoising process at different stages. Our proposed combination method amalgamates various visual conditions with greater granularity, effectively balancing the conflicts between disparate visual control information, and facilitating complementary control of high- and low-frequency information within the temporal domain. It is worth noting that when operating under a single visual condition control, our proposed method effectively reverts to the single visual control scheme. The efficacy of ControlNet’s single visual condition control has been extensively validated in numerous studies [27, 49, 51]. Therefore, this paper does not investigate the generative capabilities of our method under single visual condition scenarios. Our main contributions are summarized as follows:

- **New Insight:** We reveal that current multi-visual condition control methods perform poorly in terms of generation quality and controllability, making it difficult for generated images to align with various visual conditions and lacking effective solutions for improvement.
- **Efficient Patch Adaptation:** We propose PixelPonder, a novel mechanism which can refine the combination of multi-visual conditions by transitioning from the image level to the patch level, thereby enabling finer-grained controllable generation.
- **Flexible Condition Combination:** Our PixelPonder supports flexible visual control combinations, regardless of the category of visual control, addressing the control conflict of multiple visual conditions for the same object.
- **Promising Results:** We provide a consolidated and public evaluation of controllability and fidelity under various conditional controls, and demonstrate that PixelPonder comprehensively outperforms existing methods.

2. Related Work

2.1. Diffusion-based Generative Models

Diffusion models [5, 15, 24, 26, 29, 36] have made remarkable strides in the field of image generation. Thanks to improvements in training and sampling strategies [15, 37, 38], as well as the application of latent diffusion methods [32], the computational resources required for these models to generate high-quality images have been substantially reduced, demonstrating promising prospects in various applications [2, 4, 12, 30]. In the domain of text-to-image generation, diffusion models [32] combined with U-Net [33] have successfully integrated text control into the image generation process through cross-attention mechanisms. To fur-

ther enhance generative capabilities, the Transformer architecture has been integrated into diffusion models [6, 10, 25] to replace U-Net. Building on this foundation, FLUX [19], which introduces flow matching objectives, has achieved state-of-the-art performance in image generation.

2.2. Controllable Text-to-Image Diffusion Models

The generation of images controlled by textual descriptions often lacks fine-grained spatial control. To enhance spatial control capabilities, numerous studies [8, 17, 21, 22, 46, 49, 50] have focused on incorporating visual control signals into the generation process. In this context, ControlNet [49] proposed a network architecture consistent with the backbone network, encoding additional visual conditions into latent representations and injecting control signals into the corresponding backbone network using zero convolution, thus achieving a spatial alignment mechanism within diffusion models. Due to its straightforward approach and effective control results, it has been widely adopted in various text-to-image diffusion models [19, 32]. Furthermore, recent research has used various prompt engineering techniques [21, 46] and inter-attention constraints [7, 44] to facilitate more orderly generation.

Some studies [1, 22, 27, 42] have addressed the differences and diversity of various visual conditions in different modalities using the mix of experts (MOE) to decouple different visual conditions into distinct feature subspaces, thus establishing a unified visual control architecture. Subsequently, other research has explored the possibility of generating multiple condition controls within a single diffusion model through simple feature aggregation methods [16, 51]. However, these methods are based on the low coupling of various conditions, which limits their effectiveness in tasks requiring the control of complementary conditions.

3. Method

In this paper, we introduce PixelPonder, a specialized framework for handling complex scenarios of image generation under multiple visual conditions. The pipeline of PixelPonder is demonstrated in Fig. 3. In this section, we first provide a brief overview of the previous Diffusion Transformer in Section 3.1, along with ControlNet. Then, in Section 3.2, we dive into a detailed description of the Patch Adaptation Module, which primarily focuses on the autoregressive reorganization of visual conditions at the patch level. In Section 3.3, we elaborate on the time-step awareness injection strategy and the control implementation of the control network. Finally, we summarize our training optimization objectives in Section 3.4.

3.1. Preliminary

Diffusion Transformer (DiT)[25, 41] is applied in models such as FLUX [19] and Stable Diffusion 3 [10]. Compared

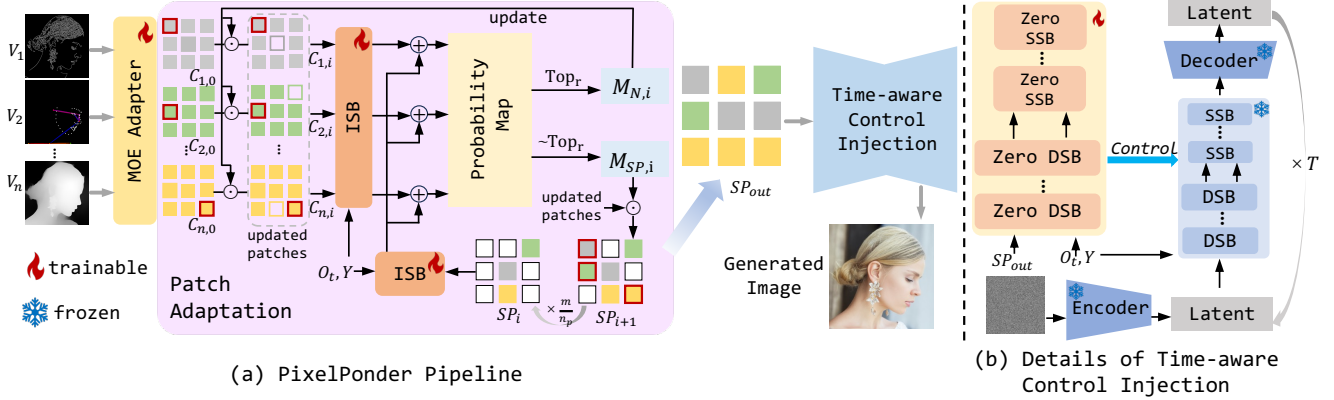


Figure 3. **Overall pipeline of the proposed PixelPonder.** The Patch Adaptation (Section 3.2) Module segments various visual conditions $\{V_1, V_2, \dots, V_n\}$ into patches and dynamically reorganizes the visual conditions at the patch level to obtain a unified visual control signal SP_{out} . Subsequently, SP_{out} is sent to the control network, with the Time-aware Control Injection scheme (Section 3.3) to achieve high-quality image generation under multiple visual conditions.

to the Latent Diffusion Model [32], these models utilize a transformer [34] instead of U-Net as the denoising network to iteratively process noise tokens.

A model with a DiT architecture handles noisy image tokens $X \in \mathbb{R}^{N \times d}$ and text condition tokens $Y \in \mathbb{R}^{M \times d}$, where d is the dimension of the embedding layer, N and M represent the number of tokens for images and text, respectively. In this structure, these tokens maintain consistent sizes before and after being processed by the transformer. Additionally, they redefine the mapping from images to noise using flow matching. In this rectified mapping, the data at time t , denoted as z_t , is transformed from the real image $x_0 \in \mathbb{R}^{C \times H \times W}$ to pure noise $N \sim \mathcal{N}(0, I)$ at the following position:

$$z_t = (1 - t)x_0 + tN, \quad (1)$$

$$\vec{V} : \mathcal{N} \rightarrow \mathcal{Z}, \quad (2)$$

where \mathcal{N} represents the spatial distribution of noisy images. \mathcal{Z} represents the spatial distribution of real images. \vec{V} is the vector field from \mathcal{N} to \mathcal{Z} .

In FLUX, a series of flow matching modules are included, among which the denoising backbone network consists of the Double Stream Block (DSB) and the Single Stream Block (SSB).

ControlNet [49] is designed to inject visual control information into a denoising network, thereby guiding the iterative process of noise tokens. Specifically, ControlNet freezes the parameters Θ of the backbone network $F(\cdot; \Theta)$ and creates a trainable copy Θ_c of these parameters to incorporate zero-initialized convolutional layers Z . When applied to generative models based on the U-Net architecture, a common practice is to add the visual condition C_i to the noise x_t as input to the trainable copy, while utilizing other signals s that is consistent with the backbone network. This process can be formalized as follows:

$$y = F(x_t, s, \Theta) + Z(F(x_t + M(C_1, \dots, C_n), s, \Theta_c)), \quad (3)$$

where M serves as a unified representation of various visual condition fusion methods, n represents the category id.

3.2. Patch Adaptation

The Patch Adaptation Module (PAM) aims to recombine various visual conditions at the patch level into a unified visual condition. This is achieved through an autoregressive iterative combination process that combines patches between different visual conditions. The specific algorithm flow of PAM is shown in Algorithm 1.

Specifically, at time step t , the PAM initializes a zero vector unified control condition $SP_0 \in \mathbb{R}^{N \times d}$ to obtain the final unified visual control combination output SP_{out} . The combination selection is defined as an update process U_i from SP_i to SP_{i+1} , with i representing the index of the number of iterations in the update process. This iterative update process can be formalized as follows:

$$SP_{i+1} = U(SP_i, \dots, O_t), \quad (4)$$

where O_t refers to the time step information, and its specific role will be discussed in Section 3.3.

Assuming that the visual input to the PAM consists of N types of condition images, denoted as V_1, V_2, \dots, V_n , we use the corresponding visual condition feature encoders E_i to obtain various visual condition features $\mathcal{C} = \{C_1, C_2, \dots, C_n\}$, $C_k \in \mathbb{R}^{e \times d}$ and e denotes the feature dimension. To analyze and process the visual condition features in a more fine-grained manner, we can consider the visual condition feature C_i as represented by patches $P_i^m \in \mathbb{R}^d$, expressed as:

$$C_k = [P_i^0, \dots, P_i^m], \quad (5)$$

where P refers to a patch, k denotes the random category id, and m denotes the number of patches.

In an update process U_i , the PAM selects a set $\mathcal{P}_i = \{P_{n,i}^s\}$ composed of multiple patches $P_{n,i}^s$ from various vi-

Algorithm 1 Patch Adaptation

Input: visual condition features $C_n \in \mathbb{R}^{N \times d}$, time step information O_t and textual feature Y .

Output: the unified visual control SP_{out}

```

1:  $SP_0 = \mathbf{0}_{N \times d}$ 
2:  $C_n = [P_n^0, \dots, P_n^m]$ 
3:  $C_0 = \{C_1, C_2, \dots, C_n\}$ 
4:  $i \leftarrow 0$ 
5:  $n_p \leftarrow$  number of selected patches
6: while  $i \cdot n_p < m$  do
7:   // The loop of process to update  $U_i$ 
8:    $M_{prob} = [\text{ISB}_C(C_i, O_t, Y)] + \text{ISB}_{SP}(SP_i)$ 
9:   // The patch selection process, denoted as  $F_{sp}$ .
10:   $M_{N,i} = \text{Zero}(\text{Top}_r(M_{prob}))$ ,  $M_{sp,i} = \sim M_{N,i}$ 
11:   $C_{i+1} = C_i M_{N,i}$ 
12:   $SP_{i+1} = SP_i + M_{sp,i} C_i$ 
13:   $i \leftarrow i + 1$ 
14: end while
15: return  $SP_i$ 

```

sual characteristics C_i . For convenience, we define this selection process as F_{sp} . The composition of this set \mathcal{P}_i considers two aspects of information: **a) The dominant role of textual information Y in the current time step in image generation**, and **b) The influence of previously selected patches $\mathcal{P}_0, \dots, \mathcal{P}_{i-1}$ on the overall composition of image control**. The update process from SP_i to SP_{i+1} can be more specifically expressed as:

$$U_i(SP_i, \dots, O_t) = SP_i + \mathcal{P}_i, \quad (6)$$

$$\mathcal{P}_i = F_{sp}(C_i, \mathcal{P}_0, \dots, \mathcal{P}_{i-1}, O_t, Y). \quad (7)$$

Specifically, to achieve F_{sp} , we design the Image Stream Block (**ISB**). Unlike DSB, to ensure that the textual control signal remains highly consistent globally, we change the DSB text input selection strategy, abandoning the textual information Y_{DSB} generated in dual-stream matching as input and instead using a globally unified textual feature representation Y as the input textual information. The ISB is used to obtain the weights of each patch in various visual condition features under the current textual control Y at time step t , denoted as $\mathcal{W}_c = \{W_{0,i}, \dots, W_{n,i}\}$. Furthermore, to meet requirement **b)** of F_{sp} , we apply an ISB to SP_i outside of C_i to obtain a global weight W_{sp} that represents the global composition information of SP_i under the current U_i . The final obtained patch selection probability map M_{prob} is given by:

$$M_{prob} = [\mathcal{W}_c] + W_{sp}, \quad (8)$$

$$\mathcal{W}_c = \text{ISB}_C(C_i, O_t, Y), \quad W_{sp} = \text{ISB}_{SP}(SP_i, O_t, Y). \quad (9)$$

In each iteration, to mask the influence of previously selected patch blocks $\{P_0, \dots, P_{i-1}\}$ on the combination selection process U_i , we use a binary mask $M_{k,i}$ to update

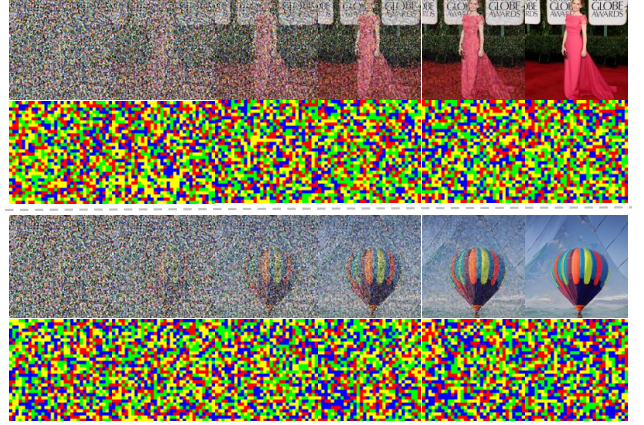


Figure 4. **Denoising results at steps 1, 5, 10, 15, 20, and 25**, where each pair includes the generated result and the selection results SP_{out} at the current time step. In each SP_{out} , canny, pose, depth and sketch are indicated in **red**, **blue**, **green**, and **yellow** respectively.

C_k^{i-1} to obtain C_k^i . The binary mask $M_{k,i}$ is derived from M_{prob} :

$$M_{N,i} = \text{Zero}(\text{Top}_r(M_{prob})), \quad (10)$$

$$\left[\bigcup_{k=1}^N M_{k,i} \right] = M_{N,i}, \quad (11)$$

where Top_r retrieves the positions of the top r patches with the highest probabilities in M_{prob} , and Zero sets the corresponding positions in the binary mask to zero.

Fig. 4 illustrates the visualization results of SP_{out} obtained by PAM in different time steps, as well as the generated images. In the early stages of the denoising process, the generated images exhibit a noticeable tendency towards patchiness. The segmentation contours between the generated image patches are prominent and remain evident even in the later stages of denoising. Both examples in Fig. 4 demonstrate the characteristics of PAM: a) PAM exhibits a balanced tendency in its selections over various time steps. b) Notably, for patches at the same location, PAM’s global selections are not consistent; instead, they encompass patches from all categories.

It is noted that C_n^0 is equivalent to C_n , which means that we do not process C_n in U_0 . The representation of the visual condition C_n during the iteration process is as follows:

$$C_k^i = \begin{cases} \mathbf{E}_k(V_k) & \text{if } i = 0 \\ M_{k,i} C_k^{i-1} & \text{if } i > 0. \end{cases} \quad (12)$$

While obtaining $M_{N,i}$, we can also acquire the mask $M_{sp,i}$ corresponding to the selected patch P_i during the update process U_i :

$$M_{sp,i} = \sim M_{N,i}, \mathcal{P}_i = M_{sp,i} C_i, \quad (13)$$

where \sim represents the negation operation.

3.3. Time-aware Control Injection

The time-aware control injection is designed to fully utilize the visual control effects of various visual conditions at different time steps during the denoising process. This is achieved by introducing additional temporal information O_t in the PSM at each time step, which controls the patch selection tendency in each update process U . To ensure that the patch selection tendencies in all selection processes U within a time step are consistently influenced by the temporal information, we use a unified temporal signal O_t at the current time step for control, as shown in Eq. (4).

Specifically, we introduce the time-step information O_t into the visual conditions and the global ISB module. This allows the ISB to simultaneously acquire time-step control information to obtain patch selection weights that are more aligned with the denoising temporal flow, which can be formalized as follows:

$$Control = D'(SP_{out}, Y, O_t, \Theta_c), \quad (14)$$

$$I_r = D(N, Control, Y, \Theta), \quad (15)$$

where D denotes the original model, Θ indicates the model parameters, D' refers to the control network, and Θ_c signifies the model parameters of the control network, I_r represents the generated image. Considering the large number of parameters in the model, we reduce the number of modules in the control network and align the image streams sequentially to the corresponding backbone modules.

To achieve stable control of visual composition under time awareness, we initialize the last linear layer to zero from the ControlNet and FLUX, denoted as zero-initialized Double Stream Block (**Zero DSB**) and zero-initialized Single Stream Block (**Zero SSB**), which can be formulated as:

$$Attention(Q, K, V) = Z\left(\left(\frac{QK^T}{\sqrt{d_k}}\right), V\right). \quad (16)$$

3.4. Training

Objective. Given a set of multi-visual prompts \mathcal{C} and a text prompt Y , we fine-tune our method to reconstruct the original image x . During the training process, we freeze the backbone network and only optimize the patch selection network and the zero controllable network. Our training objective combines V and V' to obtain the visual representation $V_{n \rightarrow c}$ under the visual prompts \mathcal{C} . This encourages the visual control network to learn the internal visual condition control flow V' based on the V pre-learned by the backbone network. The loss function \mathcal{L} is formalized as:

$$\mathcal{L} = \|(N - x_0) - \int_0^1 \vec{V} \oplus \vec{V}'(z_t, \mathcal{C}, Y, t) dt\|^2, \quad (17)$$

where the \oplus represents the vector sum of two fields.

4. Experiments

We validate the effectiveness of PixelPonder on the MultiGen-20M [20] and Subject-200K[40] datasets. Our evaluation primarily focuses on several leading methods, including T2I-Adapter [22], Uni-ControlNet [51], UniControl [27], and Cocktail [16] in the realm of multiple controllable text-to-image diffusion models. It should be noted that since Cocktail only supports pose maps, sketch maps, and segmentation maps, we only input pose maps and sketch maps when conducting experiments with Cocktail. Although the models of other approaches such as AnyControl [39] are public, their code cannot be successfully run after many attempts. More implementation details can be found in the supplementary material.

4.1. Main Results

Comparison of Controllability. As shown in Tab. 1, we report the controllability comparison results across different datasets, where the structural similarity index (SSIM) is employed to evaluate image consistency. Our PixelPonder surpasses other methods with improvements of 8.41% and 19.29% on two benchmark datasets, establishing a new state-of-the-art in image generation. This notable accomplishment demonstrates that PixelPonder possesses the capability to process intricate combinations of multiple spatial conditions, producing high-quality, harmonious outcomes that are well-aligned with the spatial conditions.

Comparison of Image Quality. Previous methods often encounter two primary issues when handling multiple visual control conditions: a) Coarsening of lines within the image, and b) Disappearance or distortion of the main subject. In contrast, PixelPonder, leveraging its unique architectural design, effectively avoids these issues by harmonizing multiple visual control conditions without compromising image quality. This is demonstrated by the quantitative results in Tab. 1, including significant improvements in FID (12.82 on MutiGen-20M and 20.34 on Subject-200K) and leading MUSIQ scores, and qualitative comparison in Fig. 5 further supports the effectiveness of PixelPonder in handling complex visual conditions.

Comparison of CLIP Score. To investigate the impact of additional visual controls on text adherence, Tab. 1 compares CLIP Score metric across methods under maximal visual conditional controls. The results reveal a consistent trade-off: methods with fewer visual constraints achieve higher text adherence. Specifically, PixelPonder demonstrates superior performance under full conditional control, achieving CLIP scores of 78.60 (MultiGen-20M) and 77.12 (Subject-200K), outperforming the compared methods. Although Cocktail attains higher scores (79.87 and 79.38, respectively) under significantly fewer visual constraints, the strong text adherence of Cocktail significantly compromises the consistency of its visual performance. As illustrated



Figure 5. **Visualization comparison** between official or re-implemented methods and our proposed model in different conditional controls.

Methods	Conditions	MultiGen-20M				Subject-200K			
		FID (↓)	CLIP Score (↑)	SSIM (↑)	MUSIQ (↑)	FID (↓)	CLIP Score (↑)	SSIM (↑)	MUSIQ (↑)
T2I-Adapter [22]	all	66.95	71.47	24.03	57.95	64.72	74.35	31.76	55.07
Uni-ControlNet [51]	all	32.58	78.08	29.37	65.85	44.35	77.40	37.98	66.75
UniControl [27]	all	25.15	74.09	35.58	72.05	30.95	72.96	47.31	67.50
Cocktail [16]	pose+hed	24.67	79.87	24.14	67.13	51.51	79.38	29.59	64.16
PixelPonder(Ours)	all	11.85	78.60	43.99	69.54	10.61	77.12	66.60	67.32

Table 1. **Comparison of generation quality, controllability, and text-image consistency on the MultiGen-20M [20] and Subject-200K [40] datasets.** The best and second-best results are highlighted in red and blue, respectively. “all” under the **Conditions** column represents that all conditions (canny maps, sketches, pose maps, depth maps) are used for generation.

in Fig. 5, the images generated by Cocktail exhibit pronounced issues of object loss and mutations when compared to those produced by other methods. This highlights PixelPonder’s unique capability to balance precise visual control with competitive text adherence, even under the most challenging full-condition settings.

Condition Types Comparison. To examine the effect of the number of visual control types on generation, Fig. 6 shows the visual results under various condition combinations, with qualitative evaluation metrics provided in Tab. 2. The examples in Fig. 6 highlight that single-condition control methods exhibit inconsistencies and instability in the

generated images, such as the background lotus leaves in row three, which display varying layouts and shapes under Canny, depth, and HED control. In contrast, PixelPonder maintains high consistency in visual features across all condition combinations. Furthermore, in Tab. 2, ControlNet++ shows significant fluctuations in FID and SSIM scores across the three visual conditions. In comparison, PixelPonder demonstrates minimal variation in these metrics. Notably, PixelPonder outperforms the best single-condition generation in both SSIM and FID under full-condition control, while maintaining strong performance on the MUSIQ metric.

Methods	Conditions	MultiGen-20M				Subject-200K			
		FID (↓)	CLIP Score (↑)	SSIM (↑)	MUSIQ (↑)	FID (↓)	CLIP Score (↑)	SSIM (↑)	MUSIQ (↑)
Source	-	-	80.69	-	69.30	-	76.48	-	66.96
Controlnet++ [20]	canny	17.69	80.64	36.69	65.67	20.89	79.42	43.57	67.07
Controlnet++ [20]	hed	13.93	81.07	42.12	71.22	15.67	78.37	56.21	68.27
Controlnet++ [20]	depth	17.56	81.12	27.79	71.23	24.90	80.01	32.70	69.75
Ours	canny+depth	15.99	76.52	38.53	68.26	17.04	77.46	55.67	67.22
Ours	canny+hed	17.69	76.31	38.23	67.14	16.69	77.26	55.20	66.19
Ours	canny+hed+depth	16.55	76.58	38.59	67.58	16.02	77.41	55.49	66.43
Ours	all	11.85	78.60	43.99	69.54	10.61	77.12	66.60	67.32

Table 2. **Results of combining different condition types.** A quantitative comparison with models controlled by single visual conditions and various combinations of visual conditions. “Source” refers to the original reference image.



Figure 6. **Comparison of multi-condition image generation** by PixelPonder with different combinations against single-condition image generation by ControlNet++ [20].

4.2. Ablation Study

Patch Selection. In Fig. 7, we illustrate the statistical distribution of each visual condition patch during the denoising steps. During the initial denoising stages from step 0 to 5, the denoising process comes from low-frequency regions to high-frequency regions. However, from step 5 to 25, the trend is completely opposite. This suggests that after establishing a rough layout in the initial stages, generating low-frequency or high-frequency regions does not necessarily require consistent information with the layout. On the contrary, it requires visual information from other frequencies to leave sufficient space to meet other visual requirements. More discussion is shown in the supplementary material.

Patch Size. To address the issue of overlapping in visual control signals, we propose a patch-level visual condition adaptation method. Tab. 3 presents the performance of PixelPonder under different patch sizes. The experimental results indicate that finer-grained image condition combination can better resolve conflicts among various visual elements in the visual conditions.

Patch Size	MultiGen-20M			
	FID (↓)	CLIP Score (↑)	SSIM (↑)	MUSIQ (↑)
2	11.26	78.62	43.21	69.15
4	12.80	78.24	40.73	68.43
8	13.46	78.07	39.75	68.15

Table 3. **Ablation on patch size.** We tested the impact of patch size in Patch Selection on controlling the generation.

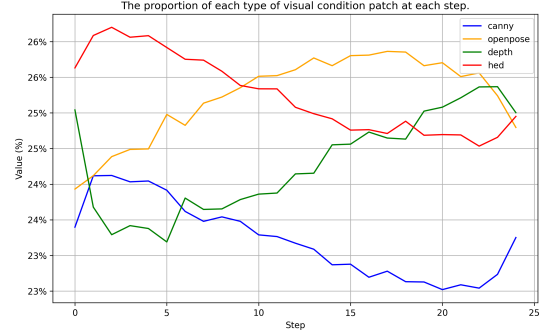


Figure 7. **Statistical distribution of each visual condition patch** during the denoising steps.

Zero	MultiGen-20M		
	FID (↓)	SSIM (↑)	MUSIQ (↑)
×	11.26	43.21	69.15
✓	11.85	43.99	69.54

Table 4. **Ablation on zero controllable flow.** × represents the non-use of zero controllable flow, while the ✓ represents the use of zero controllable flow.

Zero Controllable Flow. As shown in Tab. 4, the use of zero controllable flow significantly enhances the aesthetic quality and color richness of the images. However, this comes with a slight loss of feature consistency in the images, while maintaining better visual coherence.

5. Conclusion

In this paper, we present PixelPonder, a novel framework for compositional visual conditioning in diffusion-based image generation. Our key contribution lies in addressing the fundamental limitation of existing methods in handling conflicting guidance from multiple control signals. Specifically, we introduce two novel components, a Patch-level Adaptive Condition Adaptation mechanism that dynamically resolves spatial conflicts through learnable attention gates, and a Time-aware Control Injection scheme that orchestrates condition influence across denoising phases. Extensive experiments on several benchmarks demonstrate significant improvements over state-of-the-art methods. With PixelPonder, users can depict different aspects of objects by utilizing various visual conditions, thereby accurately realizing their various creations.

References

- [1] Omer Bar-Tal, Lior Yariv, Yaron Lipman, and Tali Dekel. Multidiffusion: Fusing diffusion paths for controlled image generation. 2023. 3
- [2] Tim Brooks, Aleksander Holynski, and Alexei A Efros. Instructpix2pix: Learning to follow image editing instructions. In *Proceedings of the IEEE/CVF Conference on Computer Vision and Pattern Recognition*, pages 18392–18402, 2023. 3
- [3] John Canny. A computational approach to edge detection. *IEEE Transactions on pattern analysis and machine intelligence*, (6):679–698, 1986. 11
- [4] Pu Cao, Feng Zhou, Qing Song, and Lu Yang. Controllable generation with text-to-image diffusion models: A survey. *arXiv preprint arXiv:2403.04279*, 2024. 2, 3
- [5] Junsong Chen, Jincheng Yu, Chongjian Ge, Lewei Yao, Enze Xie, Yue Wu, Zhongdao Wang, James Kwok, Ping Luo, Huchuan Lu, et al. Pixart-alpha: Fast training of diffusion transformer for photorealistic text-to-image synthesis. *arXiv preprint arXiv:2310.00426*, 2023. 3
- [6] Junsong Chen, Yue Wu, Simian Luo, Enze Xie, Sayak Paul, Ping Luo, Hang Zhao, and Zhenguo Li. Pixart- $\{\backslash\delta\}$: Fast and controllable image generation with latent consistency models. *arXiv preprint arXiv:2401.05252*, 2024. 3
- [7] Minghao Chen, Iro Laina, and Andrea Vedaldi. Training-free layout control with cross-attention guidance. In *Proceedings of the IEEE/CVF Winter Conference on Applications of Computer Vision*, pages 5343–5353, 2024. 3
- [8] Jiaxin Cheng, Xiao Liang, Xingjian Shi, Tong He, Tianjun Xiao, and Mu Li. Layoutdiffuse: Adapting foundational diffusion models for layout-to-image generation. *arXiv preprint arXiv:2302.08908*, 2023. 3
- [9] Prafulla Dhariwal and Alexander Nichol. Diffusion models beat gans on image synthesis. *Advances in neural information processing systems*, 34:8780–8794, 2021. 2
- [10] Patrick Esser, Sumith Kulal, Andreas Blattmann, Rahim Entezari, Jonas Müller, Harry Saini, Yam Levi, Dominik Lorenz, Axel Sauer, Frederic Boesel, et al. Scaling rectified flow transformers for high-resolution image synthesis. In *Forty-first International Conference on Machine Learning*, 2024. 3
- [11] Qingdong He, Jinlong Peng, Pengcheng Xu, Boyuan Jiang, Xiaobin Hu, Donghao Luo, Yong Liu, Yabiao Wang, Chengjie Wang, Xiangtai Li, et al. Dynamiccontrol: Adaptive condition selection for improved text-to-image generation. *arXiv preprint arXiv:2412.03255*, 2024. 2
- [12] Amir Hertz, Ron Mokady, Jay Tenenbaum, Kfir Aberman, Yael Pritch, and Daniel Cohen-Or. Prompt-to-prompt image editing with cross attention control. *arXiv preprint arXiv:2208.01626*, 2022. 3
- [13] Jack Hessel, Ari Holtzman, Maxwell Forbes, Ronan Le Bras, and Yejin Choi. Clipscore: A reference-free evaluation metric for image captioning. *arXiv preprint arXiv:2104.08718*, 2021. 11
- [14] Martin Heusel, Hubert Ramsauer, Thomas Unterthiner, Bernhard Nessler, and Sepp Hochreiter. Gans trained by a two time-scale update rule converge to a local nash equilibrium. *Advances in neural information processing systems*, 30, 2017. 11
- [15] Jonathan Ho, Ajay Jain, and Pieter Abbeel. Denoising diffusion probabilistic models. *Advances in neural information processing systems*, 33:6840–6851, 2020. 3
- [16] Minghui Hu, Jianbin Zheng, Daqing Liu, Chuanxia Zheng, Chaoyue Wang, Dacheng Tao, and Tat-Jen Cham. Cock-tail: Mixing multi-modality control for text-conditional image generation. In *Thirty-seventh Conference on Neural Information Processing Systems*, 2023. 2, 3, 6, 7
- [17] Lianghua Huang, Di Chen, Yu Liu, Yujun Shen, Deli Zhao, and Jingren Zhou. Composer: Creative and controllable image synthesis with composable conditions. *arXiv preprint arXiv:2302.09778*, 2023. 3
- [18] Junjie Ke, Qifei Wang, Yilin Wang, Peyman Milanfar, and Feng Yang. Musiq: Multi-scale image quality transformer. In *Proceedings of the IEEE/CVF international conference on computer vision*, pages 5148–5157, 2021. 11
- [19] Black Forest Labs. Flux: Official inference repository for flux.1models accessed:2024-11-12. 2024. 3
- [20] Ming Li, Taojiannan Yang, Huafeng Kuang, Jie Wu, Zhaoning Wang, Xuefeng Xiao, and Chen Chen. Controlnet ++ : Improving conditional controls with efficient consistency feedback. In *European Conference on Computer Vision*, pages 129–147. Springer, 2025. 2, 6, 7, 8, 11
- [21] Yuheng Li, Haotian Liu, Qingyang Wu, Fangzhou Mu, Jianwei Yang, Jianfeng Gao, Chunyuan Li, and Yong Jae Lee. Gligen: Open-set grounded text-to-image generation. In *Proceedings of the IEEE/CVF Conference on Computer Vision and Pattern Recognition*, pages 22511–22521, 2023. 3
- [22] Chong Mou, Xintao Wang, Liangbin Xie, Yanze Wu, Jian Zhang, Zhongang Qi, and Ying Shan. T2i-adapter: Learning adapters to dig out more controllable ability for text-to-image diffusion models. In *Proceedings of the AAAI Conference on Artificial Intelligence*, pages 4296–4304, 2024. 2, 3, 6, 7
- [23] Jiteng Mu, Nuno Vasconcelos, and Xiaolong Wang. Editar: Unified conditional generation with autoregressive models. *arXiv preprint arXiv:2501.04699*, 2025. 2
- [24] Alex Nichol, Prafulla Dhariwal, Aditya Ramesh, Pranav Shyam, Pamela Mishkin, Bob McGrew, Ilya Sutskever, and Mark Chen. Glide: Towards photorealistic image generation and editing with text-guided diffusion models. *arXiv preprint arXiv:2112.10741*, 2021. 3
- [25] William Peebles and Saining Xie. Scalable diffusion models with transformers. In *Proceedings of the IEEE/CVF International Conference on Computer Vision*, pages 4195–4205, 2023. 2, 3
- [26] Dustin Podell, Zion English, Kyle Lacey, Andreas Blattmann, Tim Dockhorn, Jonas Müller, Joe Penna, and Robin Rombach. Sdxl: Improving latent diffusion models for high-resolution image synthesis. *arXiv preprint arXiv:2307.01952*, 2023. 2, 3
- [27] Can Qin, Shu Zhang, Ning Yu, Yihao Feng, Xinyi Yang, Yingbo Zhou, Huan Wang, Juan Carlos Niebles, Caiming Xiong, Silvio Savarese, et al. Unicontrol: A unified diffusion model for controllable visual generation in the wild. *arXiv preprint arXiv:2305.11147*, 2023. 2, 3, 6, 7

- [28] Alec Radford, Jong Wook Kim, Chris Hallacy, Aditya Ramesh, Gabriel Goh, Sandhini Agarwal, Girish Sastry, Amanda Askell, Pamela Mishkin, Jack Clark, et al. Learning transferable visual models from natural language supervision. In *International conference on machine learning*, pages 8748–8763. PMLR, 2021. [11](#)
- [29] Aditya Ramesh, Mikhail Pavlov, Gabriel Goh, Scott Gray, Chelsea Voss, Alec Radford, Mark Chen, and Ilya Sutskever. Zero-shot text-to-image generation. In *International conference on machine learning*, pages 8821–8831. Pmlr, 2021. [2](#), [3](#)
- [30] Aditya Ramesh, Prafulla Dhariwal, Alex Nichol, Casey Chu, and Mark Chen. Hierarchical text-conditional image generation with clip latents. *arXiv preprint arXiv:2204.06125*, 1(2):3, 2022. [2](#), [3](#)
- [31] René Ranftl, Katrin Lasinger, David Hafner, Konrad Schindler, and Vladlen Koltun. Towards robust monocular depth estimation: Mixing datasets for zero-shot cross-dataset transfer. *IEEE transactions on pattern analysis and machine intelligence*, 44(3):1623–1637, 2020. [11](#)
- [32] Robin Rombach, Andreas Blattmann, Dominik Lorenz, Patrick Esser, and Björn Ommer. High-resolution image synthesis with latent diffusion models. In *Proceedings of the IEEE/CVF conference on computer vision and pattern recognition*, pages 10684–10695, 2022. [2](#), [3](#), [4](#)
- [33] Olaf Ronneberger, Philipp Fischer, and Thomas Brox. U-net: Convolutional networks for biomedical image segmentation. In *Medical image computing and computer-assisted intervention—MICCAI 2015: 18th international conference, Munich, Germany, October 5-9, 2015, proceedings, part III 18*, pages 234–241. Springer, 2015. [3](#)
- [34] Ludan Ruan, Yiyang Ma, Huan Yang, Huiguo He, Bei Liu, Jianlong Fu, Nicholas Jing Yuan, Qin Jin, and Baining Guo. Mm-diffusion: Learning multi-modal diffusion models for joint audio and video generation. In *Proceedings of the IEEE/CVF Conference on Computer Vision and Pattern Recognition*, pages 10219–10228, 2023. [4](#)
- [35] Chenyang Si, Ziqi Huang, Yuming Jiang, and Ziwei Liu. Freeu: Free lunch in diffusion u-net. In *Proceedings of the IEEE/CVF Conference on Computer Vision and Pattern Recognition*, pages 4733–4743, 2024. [2](#)
- [36] Jascha Sohl-Dickstein, Eric Weiss, Niru Maheswaranathan, and Surya Ganguli. Deep unsupervised learning using nonequilibrium thermodynamics. In *International conference on machine learning*, pages 2256–2265. PMLR, 2015. [3](#)
- [37] Jiaming Song, Chenlin Meng, and Stefano Ermon. Denoising diffusion implicit models. *arXiv preprint arXiv:2010.02502*, 2020. [3](#)
- [38] Yang Song, Jascha Sohl-Dickstein, Diederik P Kingma, Abhishek Kumar, Stefano Ermon, and Ben Poole. Score-based generative modeling through stochastic differential equations. *arXiv preprint arXiv:2011.13456*, 2020. [3](#)
- [39] Yanan Sun, Yanchen Liu, Yin hao Tang, Wenjie Pei, and Kai Chen. Anycontrol: Create your artwork with versatile control on text-to-image generation. *arXiv preprint arXiv:2406.18958*, 2024. [6](#)
- [40] Zhenxiong Tan, Songhua Liu, Xingyi Yang, Qiaochu Xue, and Xinchao Wang. Ominicontrol: Minimal and universal control for diffusion transformer. *arXiv preprint arXiv:2411.15098*, 2024. [6](#), [7](#), [11](#)
- [41] A Vaswani. Attention is all you need. *Advances in Neural Information Processing Systems*, 2017. [3](#)
- [42] Xudong Wang, Trevor Darrell, Sai Saketh Rambhatla, Rohit Girdhar, and Ishan Misra. Instancediffusion: Instance-level control for image generation. In *Proceedings of the IEEE/CVF Conference on Computer Vision and Pattern Recognition*, pages 6232–6242, 2024. [3](#)
- [43] Zhou Wang, Alan C Bovik, Hamid R Sheikh, and Eero P Simoncelli. Image quality assessment: from error visibility to structural similarity. *IEEE transactions on image processing*, 13(4):600–612, 2004. [11](#)
- [44] Jinheng Xie, Yuexiang Li, Yawen Huang, Haozhe Liu, Wentian Zhang, Yefeng Zheng, and Mike Zheng Shou. Boxdiff: Text-to-image synthesis with training-free box-constrained diffusion. In *Proceedings of the IEEE/CVF International Conference on Computer Vision*, pages 7452–7461, 2023. [3](#)
- [45] Saining Xie and Zhuowen Tu. Holistically-nested edge detection. In *Proceedings of the IEEE international conference on computer vision*, pages 1395–1403, 2015. [11](#)
- [46] Zhengyuan Yang, Jianfeng Wang, Zhe Gan, Linjie Li, Kevin Lin, Chenfei Wu, Nan Duan, Zicheng Liu, Ce Liu, Michael Zeng, et al. Reco: Region-controlled text-to-image generation. In *Proceedings of the IEEE/CVF Conference on Computer Vision and Pattern Recognition*, pages 14246–14255, 2023. [3](#)
- [47] Zhendong Yang, Ailing Zeng, Chun Yuan, and Yu Li. Effective whole-body pose estimation with two-stages distillation. In *Proceedings of the IEEE/CVF International Conference on Computer Vision*, pages 4210–4220, 2023. [11](#)
- [48] Hu Ye, Jun Zhang, Sibol Liu, Xiao Han, and Wei Yang. Ip-adapter: Text compatible image prompt adapter for text-to-image diffusion models. *arXiv preprint arXiv:2308.06721*, 2023. [2](#)
- [49] Lvmin Zhang, Anyi Rao, and Maneesh Agrawala. Adding conditional control to text-to-image diffusion models. In *Proceedings of the IEEE/CVF International Conference on Computer Vision*, pages 3836–3847, 2023. [2](#), [3](#), [4](#)
- [50] Tianjun Zhang, Yi Zhang, Vibhav Vineet, Neel Joshi, and Xin Wang. Controllable text-to-image generation with gpt-4. *arXiv preprint arXiv:2305.18583*, 2023. [3](#)
- [51] Shihao Zhao, Dongdong Chen, Yen-Chun Chen, Jianmin Bao, Shaozhe Hao, Lu Yuan, and Kwan-Yee K Wong. Uni-controlnet: All-in-one control to text-to-image diffusion models. *Advances in Neural Information Processing Systems*, 36, 2024. [1](#), [2](#), [3](#), [6](#), [7](#)



PixelPonder: Dynamic Patch Adaptation for Enhanced Multi-Conditional Text-to-Image Generation

Supplementary Material

The supplementary material presents the following sections to strengthen the main manuscript:

- Implementation details.
- More experiments about scale study.
- Patch Selection Analysis
- Generation Stability Comparison
- Image Consistency Exploration
- More qualitative results.

A1. Implementation Details

Dataset. Our training dataset is randomly sampled from the MultiGen-20M [20] dataset, resulting in a training set of 2.5 million samples. Each training sample contains an input image x , a text prompt, and a set of visual conditions $\mathcal{C} = \{C_1, C_2, \dots, C_n\}$. This set \mathcal{C} of visual conditions includes various types of visual cues, such as canny maps, sketches, depth maps, and pose maps, obtained from several other methods [3, 31, 45, 47]. In the testing dataset, due to the small size of the MultiGen-20M test set, and to ensure fairness in comparison, we combine the test and validation sets of MultiGen-20M to form a test set of up to 5,500 text-image pairs. Additionally, to increase the confidence in our conclusions, we randomly sample 5,000 text-image pairs from the Subject-200K[40] dataset as a second test set. This dataset provides more complex text compared to MultiGen-20M, and the Subject-200Ks in each image are clearly defined.

Training Setting. We conduct the training on 24 Nvidia V100 GPUs, using a batch size of 3 for every 3 GPUs, for a total of 200,000 training steps. The AdamW optimizer is employed with a learning rate of 2×10^{-5} . The default setting for patch size is 2, and the default number of patches selected per U_i is set to $\frac{W}{\text{patch size}}$ (where W is the width of the image features). The default depth of the ISB module is 1, and the default number of Zero DSBs and Zero SSBs is set to 2 and 4, respectively. During training, we randomly select 3 out of 4 types of conditions (canny maps, depth maps, sketch maps, and pose maps) as visual control inputs. Regarding the pose condition, since not all images contain humans, we do not discard the pose condition to ensure its effective training.

Inference Setting. During the inference process, the sampling step for PixelPonder is set to 25. For the comparative experiments with other methods, such as UnicontrolNet and Cocktail, the hyperparameters during inference is set to the official default configurations. In all visual displays except

for the multiple generated images of the same object, the global random seed is set to 100. It is worth mentioning that assuming the visual conditions consist of $H \times W$ tokens, the number of patches selected in each update process U_i is W , and the total number of update processes is H .

Evaluation Metrics. For multi-visual condition control tasks, we evaluate generation quality, controllability, and text-image consistency using a comprehensive set of mathematical and model-based metrics. **Generation quality** is assessed through FID[14] and MUSIQ [18]. FID, a model-based metric, quantifies the similarity between feature distributions of real and generated images, providing a robust measure of image fidelity. MUSIQ, another perceptual model-based metric, evaluates image quality from a human perceptual perspective by capturing both local and global quality attributes. **Controllability** is measured using SSIM [43], a mathematically grounded metric that computes the structural similarity between reference and generated images, offering a precise assessment of visual fidelity. Finally, **text-image consistency** is evaluated via CLIP Score [13, 28], a model-based metric that measures the semantic alignment between input text and generated images.

A2. Scale Study

To investigate whether PixelPonder demonstrates better image quality with larger parameter scales and training datasets, we evaluated the fidelity and consistency of the generated images using FID, SSIM and MUSIQ on different data scales and module depths.

Data Scale. We evaluate the performance of PixelPonder on different scales of training datasets, with the results shown in Tab. A1. Due to limitations in computational resources and time, we only explored up to 2.5 million data. As shown in the table, PixelPonder demonstrates significant improvements in FID and SSIM as the scale of the training dataset increases. However, MUSIQ, constrained by the original reference images, does not show further improvement after a substantial increase in the size of the data set. Compared to other methods, such as ControlNet++ and UniControl, our method achieves results comparable to those obtained by tens of millions of training samples, while being trained on only millions of samples. This indicates that there is still room for improvement in the precise control capabilities of PixelPonder.

Data scale	MultiGen-20M		
	FID (↓)	SSIM (↑)	MUSIQ (↑)
105k	12.20	40.79	68.93
686k	11.43	41.13	69.16
2.5m	11.26	43.21	69.15

Table A1. **Ablation on data scale.** FID, SSIM and MUSIQ are reported on MultiGen-20M datasets. k represents thousand, and m represents million.

A3. Patch Selection Analysis

To further explore the specific internal processes of patch selection, we conduct some investigations, including the selection tendencies of patch selection for various visual conditions, as well as the characteristics of the denoising process based on patch selection.

Previous methods exhibit a progression of features from coarse to fine during the denoising process. Specifically, generative models first create the rough outlines and layouts of various objects, followed by the addition of details, which means generating from low-frequency regions to high-frequency regions. Generally, we believe that generating low-frequency visual elements requires low-frequency information, while high-frequency visual elements require high-frequency information.

Fourier	MultiGen-20M		
	FID (↓)	SSIM (↑)	MUSIQ (↑)
×	12.79	44.97	68.38
✓	13.21	44.49	68.09

Table A2. **Ablation on fourier.** × represents the non-use of fourier, while the ✓ represents the use of fourier.

To further validate our idea, we design a Fourier-based low-frequency and high-frequency signal correction, aiming at adjusting the intensity of low-frequency and high-frequency signals to be consistent with previous conclusions. Its mathematical form is as follows:

$$f_{low} = \alpha M_{low} f t \quad (18)$$

$$f_{high} = \frac{\tilde{M}_{low} f}{\min(t, \frac{2}{3})} \quad (19)$$

where t is the current time step, M_{low} is a low-frequency mask, \tilde{M}_{low} is a high-frequency mask, α is the correction hyperparameter, f is the spectrogram, and f_{low} and f_{high} represent the corrected low-frequency and high-frequency signals, respectively. f_{low} decreases over time steps, while f_{high} increases. We incorporate this Fourier correction into the control network, and the results are shown in Tab. A2. It demonstrates that the image quality generated by the

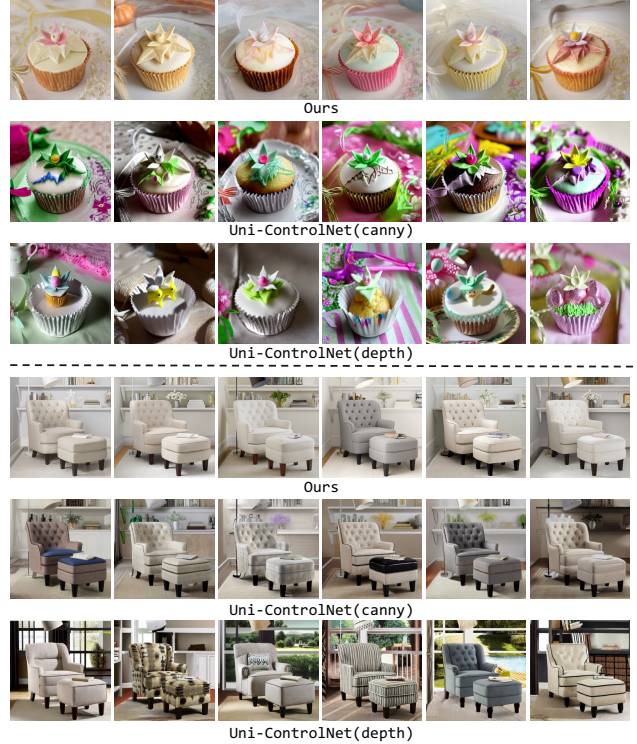


Figure A1. **Comparison of multiple random generations under single-condition and multi-condition.** *Ours* employs all available conditions, whereas *canny* and *depth* denote the use of only the canny or depth conditions, respectively.

Fourier correction constructed under the previous conclusions has declined in various aspects, which indirectly supports the validity of our conclusions.

In the two examples shown in Fig. 4, due to the fine-grained division of patches, the pose maps are mostly blank noise at many patch locations, resulting in a lack of control effect. However, contrary to our expectations, in the invalid areas corresponding to the pose maps, patch selection still chooses the blank noise from the pose maps to perturb the generation, which leads to better generation results. This is supported by the comparisons in Tab. 2, where the generation results under all conditional control scenarios significantly outperform other combinations of conditions, particularly in consistency evaluation metrics such as FID and SSIM. This indicates that appropriately adding noise during the denoising process does not negatively impact image generation; rather, it frees up more space for other visual condition controls to exert their influence, which is consistent with our conclusions regarding the selection tendencies of various visual conditions in patch selection.

A4. Generation Stability Comparison

As shown in Fig. A1, the previous single-condition control framework encounters significant challenges in preserv-

ing both stability and consistency regarding the detailed features and morphological characteristics of target objects across multiple generated images. Particularly in the cake and furniture scenarios, Uni-ControlNet manifests several limitations, including texture degradation, contour deformation, and background inconsistency. In stark contrast, PixelPonder demonstrates superior performance in maintaining both consistency and stability across these dimensions. A notable example can be observed in the cake scenario, where PixelPonder effectively maintains precise control over the cream’s morphological features while simultaneously ensuring consistent dimensional attributes of the cake across all generated images.

A5. Image Consistency Exploration

To investigate whether the images generated by PixelPonder are consistent with the visual control conditions in terms of visual elements, we provide additional relevant visual demonstrations in Fig. A2 and Fig. A3.

In each visual example, we present the reference along with its corresponding visual conditions. Additionally, the generated images are displayed under the visual conditions of the reference, as well as the extracted visual conditions from these generated images to investigate the consistency of each method with respect to various visual conditioning details in terms of visual fidelity and adherence to the specified conditions.

A6. More Qualitative Comparison

In Fig. A4 and Fig. A5, we present more visual results across various scenes. Previous methods do not separate multiple classes of visual conditions in visual control; instead, they inject multiple visual conditions simultaneously at a single time step, redundantly introducing visual elements of canny’s. Our proposed PixelPonder, through patch-level separation of visual conditions and temporal domain separation, avoids the generation of overlapping conflicting visual signals and achieves the injection of complementary information among various visual elements in the temporal domain, resulting in superior generation performance under multi-visual condition control.

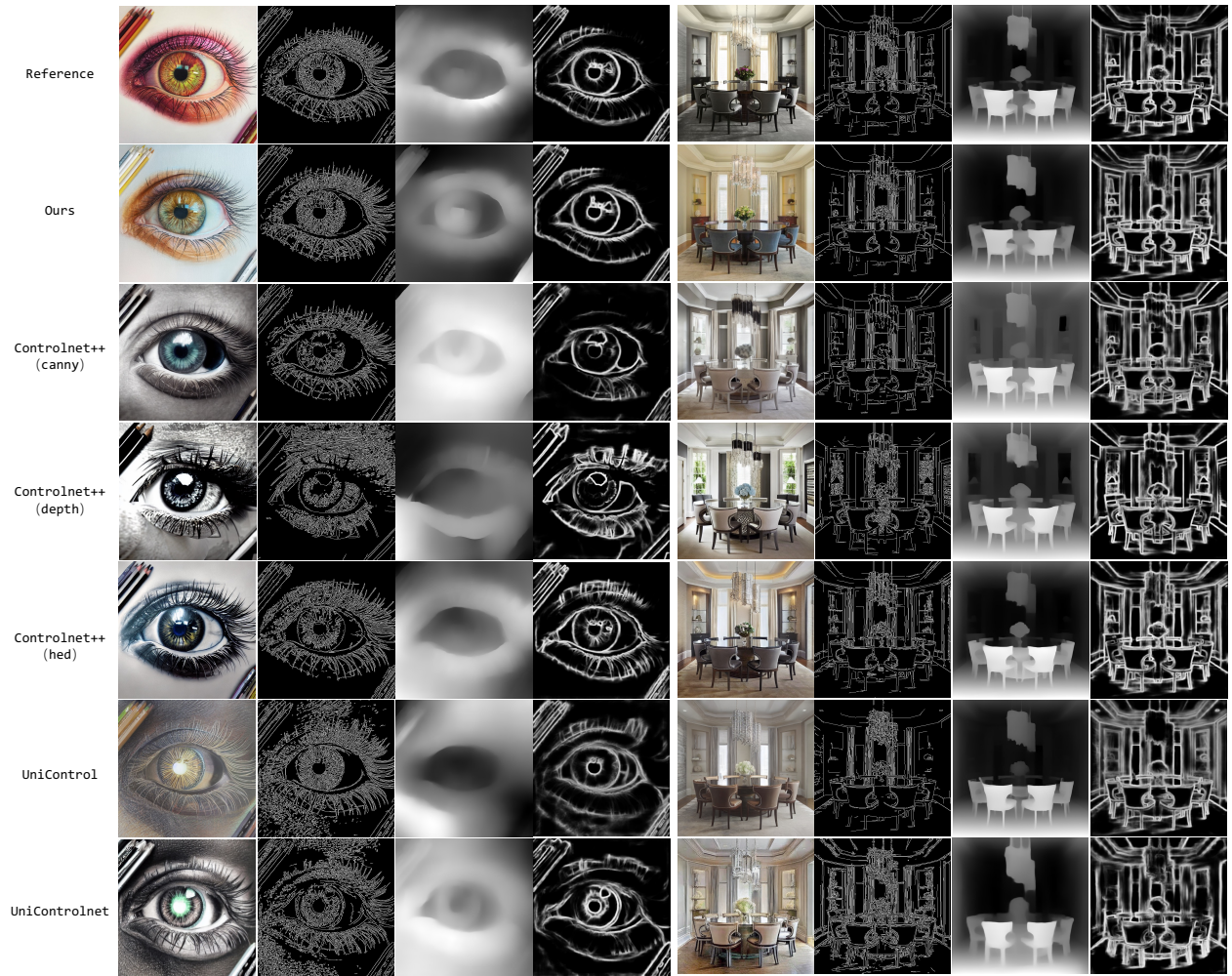


Figure A2. **Image consistency comparison** between official or re-implemented methods and our proposed model.

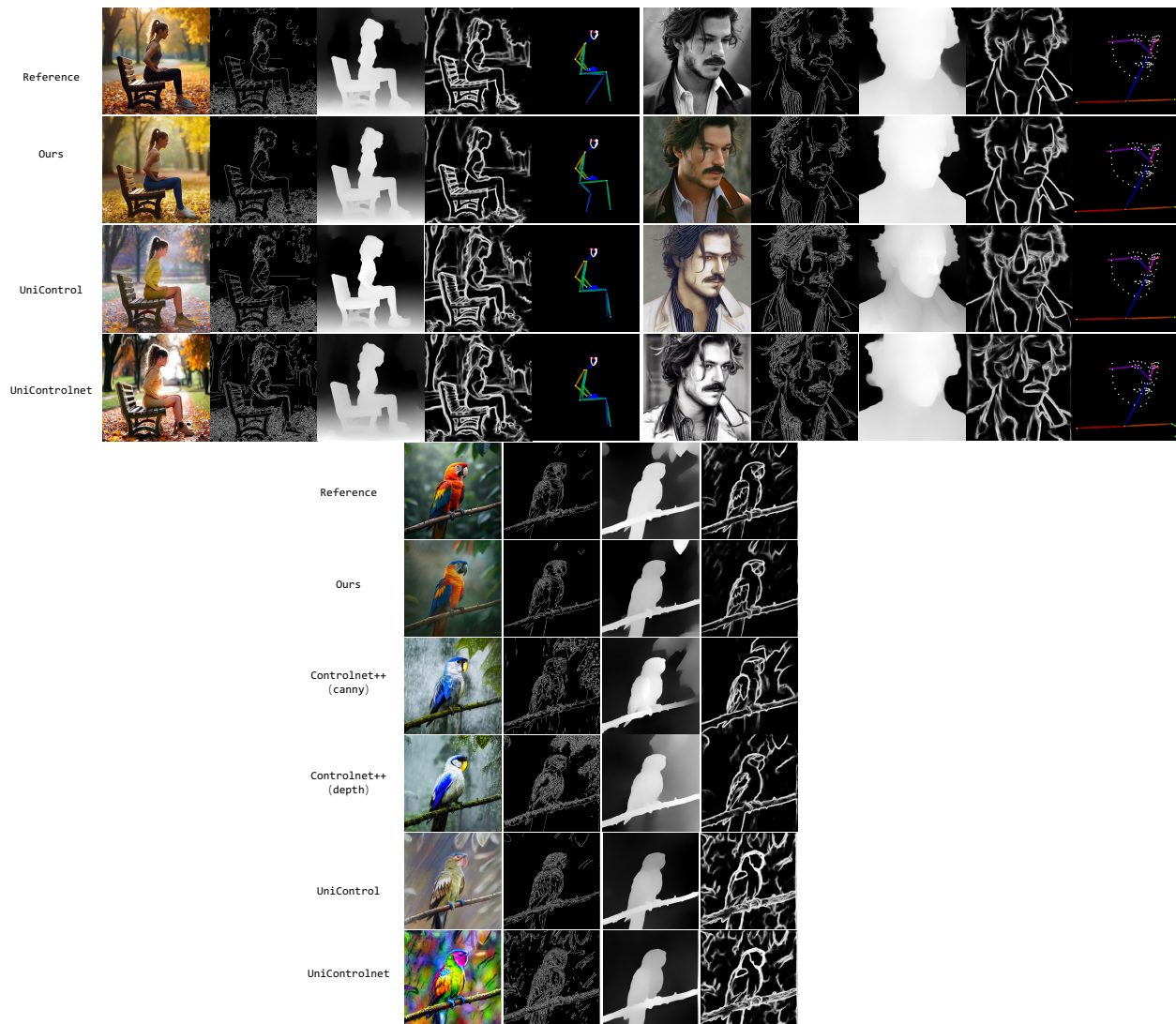


Figure A3. **Image consistency comparison** between official or re-implemented methods and our proposed model.

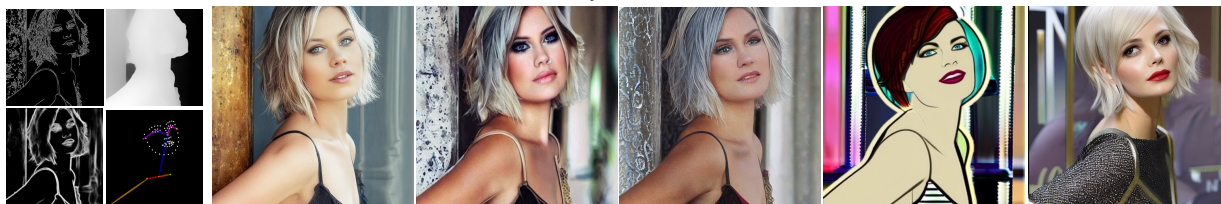
"Placed on a wooden dining table during a family breakfast, it is surrounded by plates of pancakes and fruit, basking in soft morning light."



"Amidst a snowy landscape, it rests on a rock, lightly dusted with snowflakes, with the blurred outline of a frosty pine forest in the distance."



"Undone Short Hairstyle For Fine Hair Short Hair."



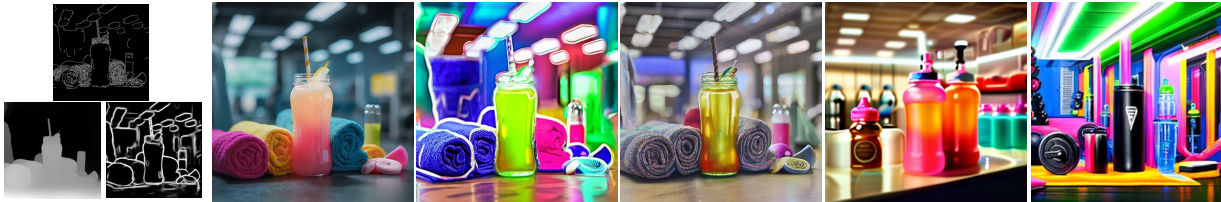
"Photo wallpaper winter, snow, nature, Dog, puppy."



"Late afternoon sunlight casts a warm glow, casting soft shadows. In the background, there is an urban cityscape with blurred figures of people walking and tall buildings capturing a cosmopolitan vibe."



"Sitting on a bustling gym counter under bright fluorescent lights, it's amongst colorful towels and water bottles, embodying the essence of post-workout refreshment."



Conditions

Ours

Uni-ControlNet

Uni-Control

T2I-Adapter

Cocktail

Figure A4. **Visualization comparison** between official or re-implemented methods and our proposed model in different conditional controls.

"On a sunny beach, the carrier rests on the sand, partially shaded by a nearby umbrella, while gentle waves roll in the distance under a clear sky."



"Solid Pine Rectangle Dining Table with several Dining Benches."



"Amid the vibrant blooms of a garden, it dangles elegantly from a low branch, the early morning dew sparkling like diamonds around it."



"Wintry sunset in Yosemite Valley. Yosemite National Park, CA."



"affordable cabinets and countertops in Atlanta."



"Pretty cat in snow."



Conditions

Ours

Uni-ControlNet

Uni-Control

T2I-Adapter

Cocktail

Figure A5. **Visualization comparison** between official or re-implemented methods and our proposed model in different conditional controls.